Preliminary Analysis of a Concept Wind Turbine Blade with Piecewise Constant Chord and Constant Twist Angle Using BEM Method

Ercan Erturk*‡

*‡Bahcesehir University, Mechatronics Engineering Department, Istanbul Turkey

Tel: +90 212 381 0866, ercan.erturk@eng.bau.edu.tr

Received: 23.07.2018 Accepted:15.08.2018

Abstract- Preliminary analysis of a concept wind turbine blade is performed using Blade Element Momentum method. The concept wind turbine blade consists of sections with constant chord and twist angle. The spanwise length of each section and the twist angle in each section is obtained numerically with using an optimization algorithm together with Blade Element Momentum theory. Using the optimization algorithm several different concept wind turbine blades are analysed using the very well-known National Renewable Energy Laboratory's Unsteady Aerodynamics Experiment Phase VI wind turbine blade geometry. The aerodynamic performances of these concept wind turbine blades are compared with the results of the original UAE Phase VI blade. The concept design offers the wind turbine blades to be manufactured easily using cheaper manufacturing techniques with the highest quality and also with the possibility of being designed as modular while having almost the same aerodynamic efficiency of a tapered and twisted wind turbine blade.

Keywords Pultruded straight wind turbine blade, sectioned wind turbine blade, BEM method, wind energy

1. Introduction

Wind is a clean and non-polluting source of renewable energy. Each year the number of installed wind turbines increases and the industry experts predict that by 2050 one third of the world's electricity needs will be fulfilled by wind power [1].

In wind turbines the rotor blades not only represent the most important part whose properties quite often determine the performance and lifetime of a turbine but also constitute the highest cost component of a wind turbine [2]. A wind turbine blade is essentially a load-carrying beam covered with an airfoil shaped shell. In order to increase the aerodynamic efficiency, the wind turbine blades are designed as twisted and tapered such that the blades have a 3-Dimensional surface from root to tip. Wind turbine blades are manufactured using composite materials and today the vacuum assisted resin transfer molding is the most widely used manufacturing method to produce wind turbine blades [3,4]. Commonly a single wind turbine blade is manufactured in steps. First the two half of a blade is molded as two aeroshells with a load-carrying box (spar). Then these two half rotors are bonded to each other together with the internal shear webs. In most of these steps usually hand laboring is used. After manufacturing, the blades are subjected to quality control [4].

During operation a wind turbine blade is subjected to considerable forces. The spar cap and the shear webs conforms the structural strength (solidity). The integrity of the wind turbine blade is highly dependent on the quality of the manufacturing and also the quality of the bonding between the shear webs and spar caps. While experiencing continual high dynamic loads the wind turbine blades can develop various different types of damage and failure modes during operation [5]. Griffin and Malkin [3] lists the manufacturing defects (e.g., wrinkles in laminate, missing or incomplete bond lines, dry fibers) as one of the leading causes of the blade failure. Considering the used manufacturing techniques of the blade it is hard to automate the blade manufacturing and obtain consistent quality in each blade. According to Sheng [6] blade replacements in the first 2 years of a wind turbine are typically due to the manufacturing defects or damage that occurs during transport and construction.

Wind turbine manufacturers are facing significant blade failure problems. Windpower Monthly magazine [7] points out that blade failures are the primary cause of insurance claims in the US onshore market and they account for over

40% of the claims. The financial consequences of catastrophic failures, extensive remediation and retrofit campaigns are considerably high. These problems cause commercial losses to both wind turbine manufacturers and wind project developers [3]. For example in 2009 a major turbine manufacturer had made a commitment of approximately $100 million for a comprehensive retrofit operation to safeguard and enhance 1251 blades around the world [8]. Windpower Monthly magazine [7] states that by the year 2015 out of 700000 blades operating worldwide, 3800 blades fail annually. As an example to the financial cost of blade replacements, for a 5MW wind turbine the replacement cost of a blade is about $391,000-$547,000 and the replacement cost of a rotor is about $1.9-$2.3 million [9].

With increasing rated powers of wind turbines, the blades gets bigger and bigger. As the blades gets bigger most critical failure modes for the blade change significantly [10]. Increasing the reliability and lifetime of wind turbine blades is an important problem for wind turbine manufacturers [11] and as the Power magazine [12] states that the blade failure rates are as high as 20% and there is a great challenge for the wind turbine blade industry in improving the manufacturing efficiency to address blade failure issues.

Today several wind turbine blade manufacturers use pultruded carbon fiber-reinforced spar caps incorporated as the reinforcing member in their wind turbine blades [13].

Pultrusion is an automated process used in production of constant cross section composites. In pultrusion process the reinforcements are drawn into a resin bath then into a shape preformer and then out to a heated die. The pultrusion process requires little labor and since the process is continuous the manufacturing is cost efficient yielding a product at just above the material cost in mass production. The process ensures repeatable consistent high quality net shape parts with high fiber volume and almost zero variability between final parts [14,15]. Compared to the current manufacturing process of composite wind turbine blades, with pultrusion manufacturing process, it is possible to overcome the manufacturing defects listed in Griffin and Malkin [3]. However in pultrusion the restriction is that the part must be constant in cross section which is a drawback in wind turbine blade applications. With pultrusion manufacturing process it is not possible to pultrude a twisted, tapered wind turbine blade.

Feasibility of using pultruded straight blades in wind turbine rotors is examined in several studies [16,17,18]. In a study Migliore and Cheney [16] studied the feasibility of using pultruded blades for a 400kW wind turbine. Migliore and Cheney [16] stated that the pultruded blades are not only lighter with significantly less weight compared to traditional blades and the cost of blades are also significantly less. In [16] Migliore and Cheney studied the aerodynamic analysis of two different blades; a straight non-tapered non-twist pultruded blade and a hybrid blade. The hybrid blade is a combination of straight non-tapered non-twist pultruded part towards the tip of the blade with a tapered hand manufactured part towards the hub of the rotor. Migliore and Cheney [16] showed that:

- With pultruded blades the weight of the rotor decreases approximately 40%
- Energy capture degrades by approximately 12% for straight pultrusions compared to blades with twist and taper.
- Energy capture degrades by approximately 5% for hybrid blades with root fairings and modular tips.
- The use of pultruded blades has the potential to significantly reduce the cost of wind turbine rotors.

Furthermore Migliore and Cheney [16] stated that rotors using pultruded blades showed exceptional reductions in rotor cost per kWh compared to rotors having conventional tapered and twisted blades.

As the results of Migliore and Cheney [16] confirms, a non-tapered and non-twist pultruded wind turbine blade suffers aerodynamic performance penalty because of the lack of twist and taper and as the blades get bigger and longer this penalty would increase. As a remedy, Migliore and Cheney [16] considered the hybrid blade. The hybrid blade consists of two parts joined together. Towards the tip, the blade is made of pultruded straight blade with no twist and no taper. Towards the root there is a part where the blade has taper but no twist. This hybrid blade can be considered as partial-tapered and non-twist blade. Although the whole hybrid blade is non-twist blade, their [16] results showed that even a partial taper helps to decrease the aerodynamic drawbacks of using a non-tapered non-twist pultruded straight blade.

In a study Lanzafame and Messina [19] have proposed a two section wind turbine blade with variable chord and no twist in each section. In their study the considered wind turbine blade consists of two sections. In each section the blade has a variable chord with constant blade angle (no twist). However the blade angles are different in the two sections. The proposed blade can be considered as a linear tapered blade with two sections having two different constant blade angles with a step change in the value at the junction of the two sections. Lanzafame and Messina [19] have simulated the performance of the proposed wind turbine blade and compared their results with that of the NREL's Unsteady Aerodynamics Experiment (UAE) Phase VI [20] wind turbine blades. Their [19] results showed that by having two different angles with a step change at the junction in a tapered but non-twist blade it is possible to decrease the aerodynamic drawbacks of having a non-twist blade.

In patent databases, a German R&D company on wind turbine blades, Smart Blade GmbH, has a patent on modular rotor blade [21]. In this design the wind turbine blade consists of longitudinal profiled sections that have two dimensional cross sections. In their design the profiled straight sections are connected to each other with an angle offset at the junctions.

As similar to the Smart Blade GmbH design, in this study we will numerically simulate and analyse the performance of a wind turbine blade that consists of several sections with constant chord length (non-tapered) and with constant twist angles (non-twist). We will first describe the concept sectioned non-tapered and non-twist blade. Then using an optimization approach we will design several

different blades with different number of sections as an alternative to the blade used in NREL's UAE Phase VI wind turbine [20]. By using a Blade Element Momentum (BEM) analysis we will compare the aerodynamic efficiency of these different sectioned blades with the original blade used in NREL's UAE Phase VI. Detailed simulation results of this concept wind turbine blade are presented.

2. Blade Element Momentum Theory Calculations

The BEM method is widely used in wind turbine blade analysis. In Blade Element Momentum Theory we basically equate the axial thrust and the torque derived from the Momentum Theory to that obtained using the Blade Element Theory. The BEM method is very well known and published in the literature (Burton et. al. [22], Manwell et. al. [23], Hansen [24]).

In BEM analysis, the axial induction parameter is defined as the following [25]

$$a = \frac{1}{1 + \frac{4F(\sin\emptyset)^2}{\frac{Nc}{2\pi r}(C_L\cos\emptyset + C_D\sin\emptyset)}} \quad (1)$$

Also the tangential induction parameter is defined as the following [25]

$$a' = \frac{1}{\frac{4F\sin\emptyset\cos\emptyset}{\frac{Nc}{2\pi r}(C_L\sin\emptyset - C_D\cos\emptyset)} - 1} \quad (2)$$

where F is Prandtl's tip loss factor and defined as

$$F = \frac{2}{\pi}\cos^{-1}\left(\exp\left(-\frac{N(R-r)}{2r\sin\emptyset}\right)\right) \quad (3)$$

Note that in the turbulent wake state, i.e. when the axial induction parameter (a) is high, the momentum theory predicts a reversal of the flow therefore the theory is no longer valid. When the axial induction parameter is greater than a critical value the Glauert empirical correction is used in our simulations as the following, if $a > a_c$

$$a = \frac{1}{2}\Big(2 + K(1-2a_c) - \sqrt{(K(1-2a_c)+2)^2 + 4(Ka_c^2 - 1)}\Big)$$

where

$$K = \frac{4F(\sin\emptyset)^2}{\frac{Nc}{2\pi r}(C_L\cos\emptyset + C_D\sin\emptyset)} \quad (4)$$

The value of a_c is taken as 0.3. The differential torque developed by the blade element is given as

$$dQ = 4\pi\rho U_\infty \Omega F a'(1-a)r^3 dr \quad (5)$$

To obtain the total torque, Ω, developed by the rotor, the above equation is integrated using the Trapezoidal rule. The power developed by the rotor is then calculated using the following equation

$$P = Q\Omega \quad (6)$$

Table 1. AERODAS parameters for NREL SERI S809 airfoil (from Spera [30])

AERODAS LIFT AND DRAG MODEL			
PARAMETERS FOR NREL SERI S809 AIRFOILS			
Constants for All Airfoils			
ACL2	41.0		
ACL3	92.0		
S2	-0.0320		
ACD2	90.0		
Constants for Specific Airfoil			
Name	S809 Smooth		
AR	10,000		
t/c	21.0		
A0	-1.0		
ACL1'	14.0		
ACD1'	20.1		
S1'	0.155		
CL1max'	1.07		
CD0	0.007		
CD1max'	0.2		
M	3.0		
F1	1.138		
G1	1.922		
Lift/Drag Model Parameters			
	Reference	Test Data	Blade
AR	10,000.00	10,000.00	15.28
1/AR	0.0001	0.0001	0.0654
S1	0.155	0.155	0.125
ACL1	14.0	14.0	15.7
ACD1	20.1	20.1	21.8
CL1max	1.07	1.07	1.047
RCL1	1.254	1.254	1.033
N1	1.85	1.85	2.01
CD1max	0.2	0.2	0.226
CL2max	1.138	1.138	1.036
RCL2	0.494	0.494	0.596
N2	3.3	3.3	2.74
CD2max	1.921	1.921	1.624

The reader is referred to Burton et. al [22], Manwell et. al. [23] and Hansen [24] for details on the BEM method.

Blade Element Momentum Theory calculations often require the lift and drag coefficients of the airfoil used in the wind turbine blade at a wide angle of attack range. There are very few experimental airfoil polar data with a wide angle of attack range (-180° to +180°) in the literature and those are only for certain airfoils. When the angle of attack is higher than the stall angle, airfoils behave like a flat plate. In the literature there are some extrapolation techniques that match the pre-stall lift and drag coefficients of the airfoils with the flat plate lift and drag coefficients after stall in order to obtain the lift and drag coefficients for a wide angle of attack range to use in BEM simulations (Viterna and Janetzke [26], Montgomerie [27], Lindenburg [28], Tangler and Kocurek [29], Spera [30])

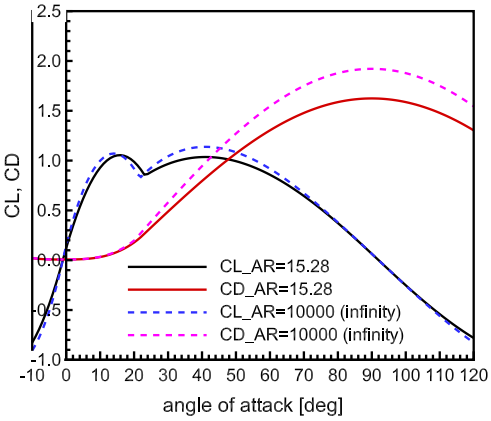

Fig. 1. Lift and Drag coefficients of S809 airfoil

In a study Spera [30] have developed AERODAS model to estimate the pre-stall and post-stall lift and drag characteristics of rotating airfoils. The model uses empirical approach and the polar coefficients are modeled by a set of algebraic equations. The algebraic equations use several parameters and if these parameters are given it is possible to reconstruct the polar data from these given parameters. Spera [30] has demonstrated the efficiency of the AERODAS model for several airfoils including NREL SERI S809 airfoil and for this particular airfoil Spera also tabulated the model parameters he used to construct the lift and drag curves. These parameters for S809 airfoil are given in Table 1 and also the constructed lift and drag curves of S809 airfoil using these parameters are given in Figure 1. In this study for S809 airfoil we use the lift and drag coefficient suggested by Spera [30]. We note that the aspect ratio of the wind turbine blade used in UAE Phase VI is 15.28. The reader is referred to Spera [30] for further details.

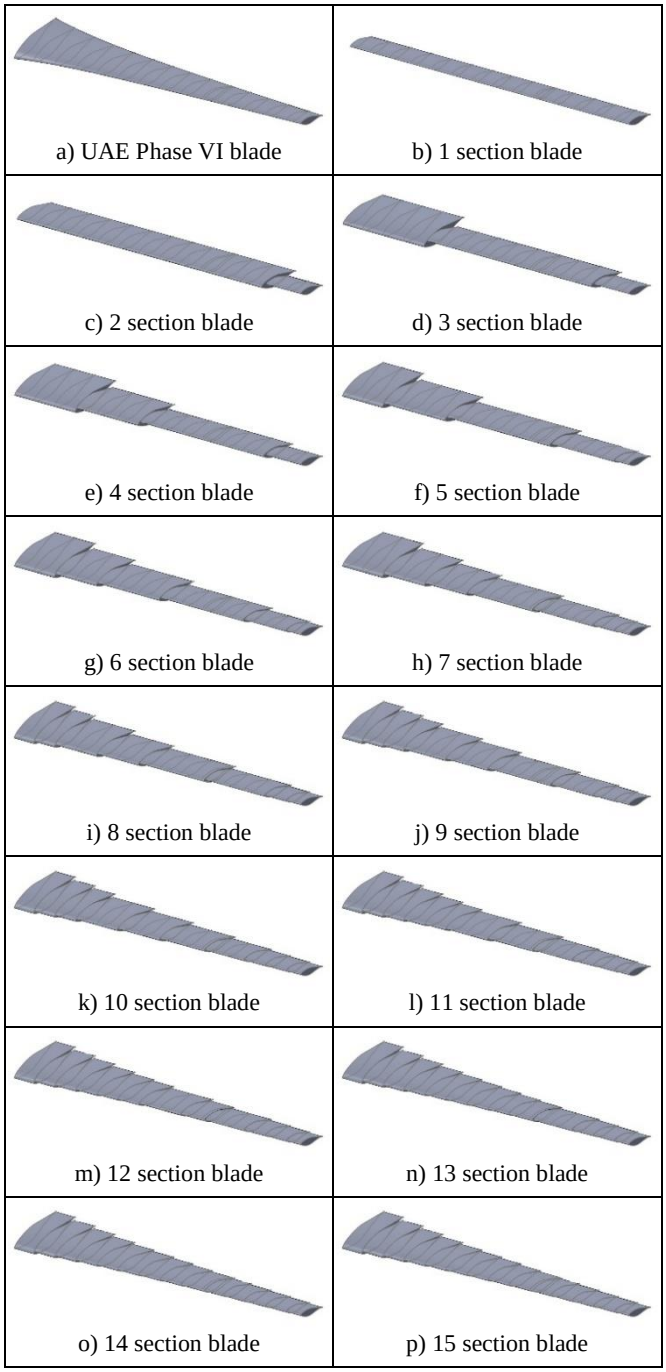

Fig. 2. Technical drawings of UAE Phase VI blade and concept blades

To help students in their research projects we have developed an interactive spreadsheet in order to use the AERODAS model easily and efficiently. With the help of this spreadsheet, the researchers can use this model by just clicking a few buttons. The "AERODAS.xls" spreadsheet is open to public (free to use) in the link given in reference [31].

In National Renewable Energy Laboratory (NREL), several combined experiments and simulations were done on wind turbines and the results are well documented. In Unsteady Aerodynamic Experiment (UAE) Phase VI, a two bladed wind turbine was tested [20]. The blades of UAE Phase VI wind turbine are twisted with having a variable chord (i.e. tapered and twisted). The blades use the NREL SERI S809 airfoil profile. The UAE Phase VI rotor was designed for a wind speed of 8 m/s and it has a rotational speed of 72 rpm. The blades have a pitch angle of 3°. The twist and chord distribution of the UAE Phase VI rotor is given in Table 2-a (Giguere and Selig [32]). In this table "Delta r" denotes the blade element thickness (i.e. length). From root to tip of the blade there are 16 stations in the blade therefore there are 15 segments (blade elements) in the blade. The technical drawing of UAE Phase VI blade is given in Figure 2-a.

Using the BEM code we developed in MATLAB and using the CL-CD values of AERODAS model for S809 airfoil shown in Figure 1 (AR=15.28), we have simulated the UAE Phase VI rotor. Figure 3 shows our computed power results along with the CER/NASA experimental results presented in Tangler [33], BEM simulation results of Spera [30] and Lanzafame and Messina [19] and CFD simulation results of Yelmule and Anjuri [34]. The data points of Tangler [33], Spera [30], Lanzafame and Messina [19] and Yelmule and Anjuri [34] are scanned from their corresponding figures, digitized and then plotted in Figure 3. As explained above in our simulations we utilize the Prandtl's approximation for the tip loss factor. In Spera [30] it is not mentioned if tip loss was used or not. In our simulations when we assume no tip loss, our results almost

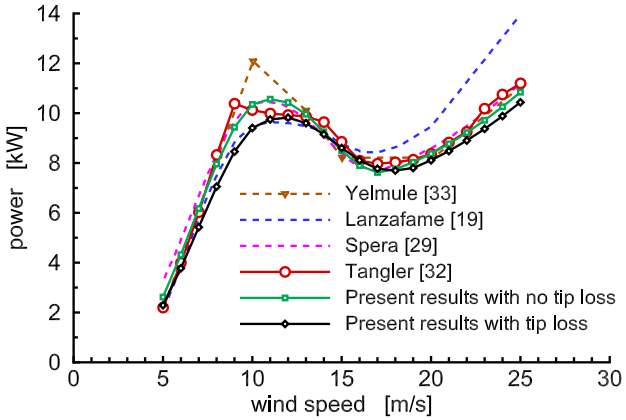

Fig. 3. UAE Phase VI wind turbine power

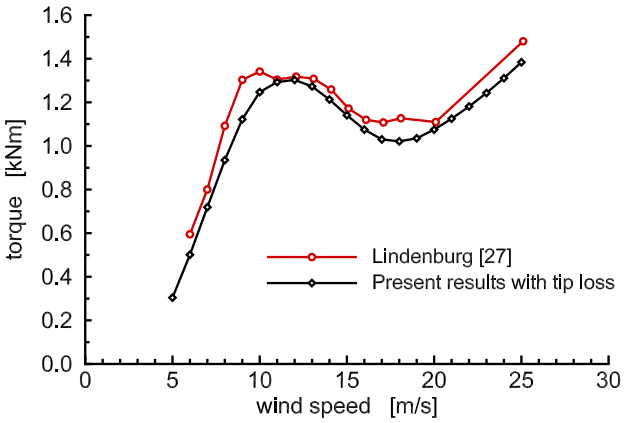

Fig. 4. UAE Phase VI wind turbine torque

match perfectly with that of Spera [30]. As seen in Figure 3 our simulation results for power agree very good with CER/NASA experimental data published in Tangler [33]. Figure 4 shows our results for torque together with the CER/NASA experimental results given in Lindenburg [28] and as it is seen in this figure the agreement is very good also. Figures 3 and 4 show that our simulation results are in very good agreement with both experimental and simulation results found in the literature.

In wind turbine blades at the design wind speed it is always preferred that the Cl/Cd ratio (glide ratio) should be high at each blade element. Table 2-a also shows our calculated angle of attack results at each station of the UAE Phase VI blade at the design wind speed at the last column. Figure 5-a shows the corresponding polar data at each station of the UAE Phase VI blade (red circle symbols) together with the lift versus drag coefficient of S809 airfoil (black line). As it is seen in this figure, in most of the stations of the UAE Phase VI blade the polar values are concentrated near the optimum (Cl/Cd)max value of S809 airfoil. This suggests that at the design conditions most of the blade elements work at the best aerodynamic condition. The angle of attack range throughout the UAE Phase VI blade given in Table 2-a is also shown as shaded area in Figure 6-a. As seen in the lift curve in Figure 6-a, anywhere on the UAE Phase VI blade the angle of attack is smaller than the stall angle such that the whole blade operates in the attached flow regime on the left side of the stall peak.

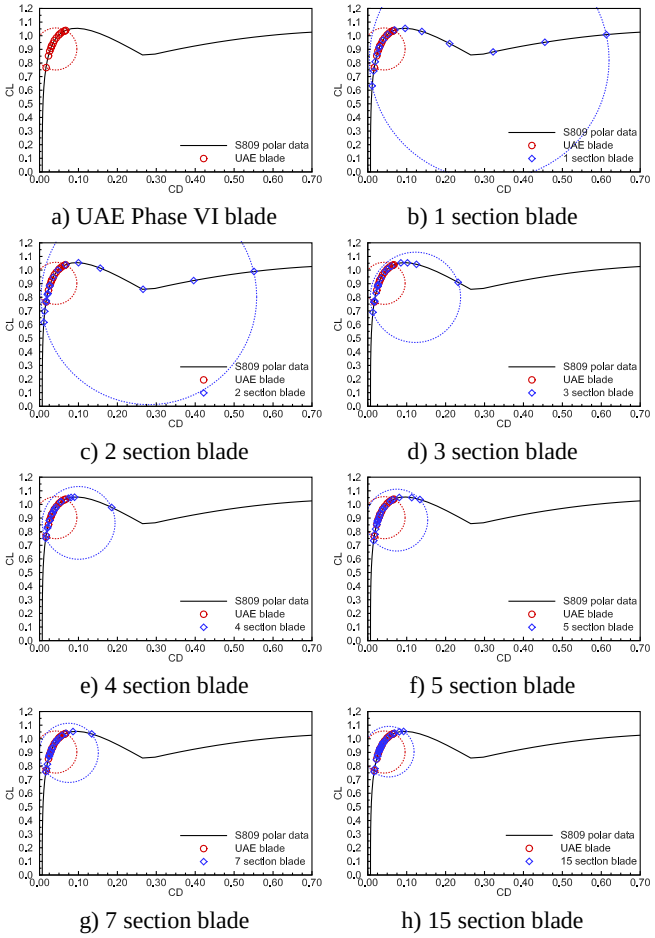

a) UAE Phase VI blade
b) 1 section blade
c) 2 section blade
d) 3 section blade
e) 4 section blade
f) 5 section blade
g) 7 section blade
h) 15 section blade

Fig. 5. Lift-drag polar curve and polar data of UAE Phase VI and concept blades

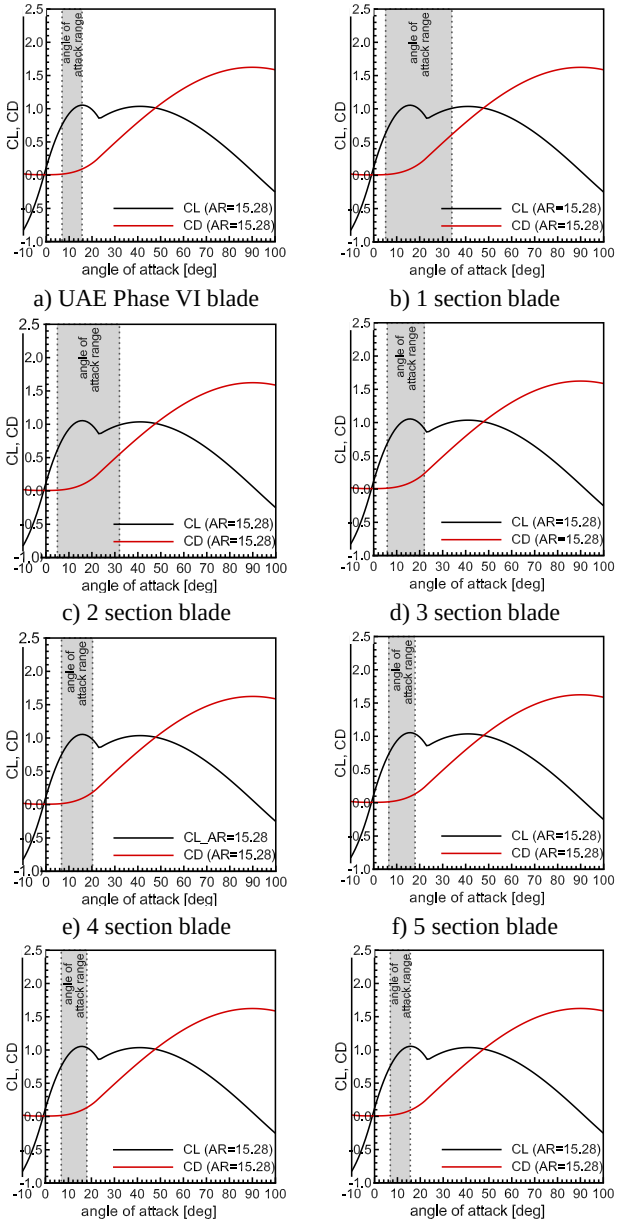

a) UAE Phase VI blade
b) 1 section blade
c) 2 section blade
d) 3 section blade
e) 4 section blade
f) 5 section blade
g) 7 section blade
h) 15 section blade

Fig. 6. Lift & drag curves of S809 airfoil and calculated angle of attack range of UAE Phase VI and concept blades

We are going to demonstrate the efficiency of the concept wind turbine blade designs by comparing it with the original UAE Phase VI wind turbine blade. We use the same design parameters for the concept blades, such as the airfoil profile is S809 airfoil profile, the design wind speed is 8m/s, the rotational speed is 72 rpm, and also the pitch angle is 3°. Also in all of our results Galeurt tip loss is utilized.

3. The Concept Wind Turbine Blade with Piecewise Constant Chord and Constant Twist Angle

In order to apply BEM method, the blade is divided into segments (blade elements) as shown in Figure 7. At each i^{th} station the BEM theory equations are solved for the axial and tangential induction parameters iteratively. Using the solved parameters together with the known parameters we then calculate torque developed by the rotor by integrating. From this, the power developed by the rotor and also the power coefficient is calculated.

A wind turbine blade should have a continuous taper and also a continuous twist along the span of the blade for the best aerodynamic efficiency such that the wind turbine blade should have a 3 dimensional surface. In their study, in a way, Lanzafame and Messina [19] have a piecewise 3-D surface on their wind turbine blade. Their considered blade has already a taper but it has no twist. However they divided the blade into two parts where each part has a different constant twist angle. Their BEM simulation show that their proposed blade has a good aerodynamic performance.

In their patent [21] Smart Blade GmbH company created a piecewise 3-D wind turbine blade with each pieces having straight sections with constant two dimensional cross sections that are connected to each other with an angle offset at the junction.

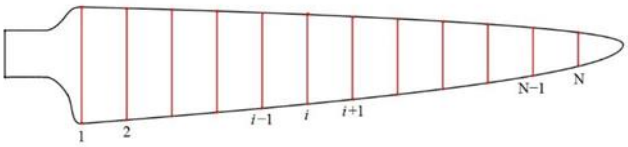

Fig. 7. Segments in tapered and twisted wind turbine blade for BEM simulation

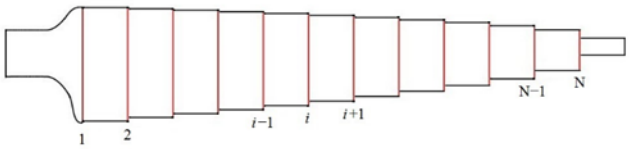

Fig. 8. Wind turbine blade with segments with constant taper and constant twist

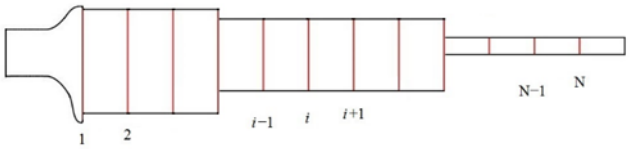

Fig. 9. Wind turbine blade with sections with many segments with constant chord and constant twist

In BEM simulations generally the blade is divided into 10~20 segments (blade elements) as illustrated in Figure 7. Applying the same idea of [21] and using constant chord and constant twist in each segment we can obtain the blade as illustrated in Figure 8. The concept blade in Figure 8 has a 3-D piecewise surface with several constant chord and twist segments. We note that in Figure 8 if infinite number of segments are used such that the spanwise length of each blade element is infinitely small, the surface of the blade will be a 3-D continuous surface. Then we group some segments and use same constant chord and constant twist in these groups as illustrated in Figure 9. We refer to these groups as "sections".

In our analysis, we will have sections in the concept wind turbine blades where in each section the chord and twist values are constant. These sections are connected to each other and at the junctions there is a step change in the chord and the twist values between the sections. Each section may have one or many segments depending on the length of the section. In order to start our analysis, first we have to choose the number of sections there is going to be in the blade. For example if we choose the blade consists of a single section, this means that all 15 segments in the blade will have the same constant chord and twist. Single section blade is a special case and it can also be named as non-tapered and non-twist blade. If we choose the blade consists of 2 sections, then this means that the blade will have a part with constant chord and twist from the root to some radial distance and from this radial distance to the tip there will be another part that has also constant chord and twist with different values. At the joint of these two sections there will be a step change in the chord and twist values. We note that since we have 15 segments in the blade, a 2 section blade can have 14 different variations in terms of the length of the sections. For example starting from the root, the first section can have 1 segment and the second section can have 14 segments. This is one possibility. Another possibility is that starting from the root the first section can have 2 segments and the second section can have 13 segments. In this case the length of the section close to the root is increased and the length of the section close to the tip is decreased accordingly. Continuing like this a two section blade can have 14 different geometry for a blade with 16 stations (15 segments) as given in Table 2-a. Continuing further, similarly we can also go ahead and choose the blade to have 3 sections. In this case there will be two joints in the blade. For the lengths of each section, there can be 91 possibilities. For example starting from the root the first section can have 1 segment, the middle section can have 1 segment and the third section close to the tip can have 13 segments. Similarly the first section can have 1 segment, the middle section can have 2 segment and the third section can have 12 segments. In a 3 piece blade we have to consider all of the 91 different possible geometries. Continuing the same way we can at most have 15 sections in a wind turbine blade with 16 stations. In this case there will be 14 joints in the blade and each section will have only 1 segment. In this study we have considered all of the options such that the blade can consist of 1 section to 15 sections and in each of these options we have considered all of the corresponding possible geometries in each case.

After choosing the number of sections, the second step is to set the constant chord and constant twist values in each section. For the constant chord values we will use the average of the chord values of the original UAE Phase VI blade in each section given in Table 2-a. We note that the chord value appears as a multiplier in the torque and power calculations and therefore directly affects the power. In our concept blades we decided that the section close to the tip will always have the chord value at the last station given in Table 2-a. This way in our concept blade we are matching the smallest chord value to the smallest chord value in the UAE Phase VI blade at the tip. In the concept blade at other sections we will set the chord value to the average chord value of the UAE Phase VI blade in the corresponding section.

In order to set the twist values in each section we will apply an optimization. For this we modified our BEM code and added an optimization algorithm that will find the best possible geometry that offers the maximum power. In this algorithm, for every section of the blade, the algorithm will change the twist value incrementally and then apply the BEM equations. Among these different twist values it will choose the value that will give the maximum power for the selected section. In the algorithm in changing the twist values incrementally we need to set the maximum and minimum values for the iteration on the twist parameter and for this again we used the twist values of the corresponding segments in the original UAE Phase VI blade given in Table 2-a such that the maximum and minimum values for the twist value iteration loop we have used the twist values at the stations at both ends of the sections.

The following pseudocode explains the algorithm in detail for easy understanding. Let us consider a blade with 3 sections such that the section close to the root has 2 segments, second and middle section has 5 segments and the third section close to the tip has 8 segments. Using the exact values listed in Table 2-a, for this specific case the algorithm looks like the following

```
chord = 0.7095 (average of 0.737 and 0.682)
set maximumsection1power = 0
    do twist = 20.05 to 9.67 with -0.01 increment
    :   do segment = 1 to 2
    :   :   apply BEM method to the segment
    :   :   calculate power for the segment
    :   end do
    :   set sum1power = power1+power2
    :   set maximumsection1power = max(sum1power , maximumsection1power)
    end do
chord = 0.612 (average of 0.682 and 0.542)
set maximumsection2power = 0
    do twist = 9.67 to 1.51 with -0.01 increment
    :   do segment = 3 to 7
    :   :   apply BEM method to the segment
    :   :   calculate power for the segment
    :   end do
    :   set sum2power = power3+power4+power5+power6+power7
    :   set maximumsection2power = max(sum2power , maximumsection2power)
    end do
chord = 0.356 (equal to the last chord value at the tip)
set maximumsection3power = 0
    do twist = 1.51 to -2.00.with -0.01 increment
    :   do segment = 8 to 15
    :   :   apply BEM method to the segment
    :   :   calculate power for the segment
    :   end do
    :   set sum3power = power8+power9+power10+power11+power12+power13+power14+power15
    :   set maximumsection3power = max(sum3power , maximumsection3power)
    end do
set totalpower = maximumsection1power+maximumsection2power+maximumsection3power
```

The above algorithm is followed for all of the 91 different possible geometries for a 3 section wind turbine blade and among all of these, the geometry that offers the most power is chosen as the concept 3 section wind turbine blade.

4. Results

Following the algorithm described above we have obtained results for the concept wind turbine blades having from 1 section to 15 section. Figure 2, 5, 6 and 10 and also Table 2 summarize the whole results obtained in this study.

Table 2 tabulates the resulting geometries of the concept wind turbine blades with chord and twist values at radial distances. After following the optimization algorithm described above and considering all of the possible different geometries, the data presented in this table offers the most power at the design wind speed for each concept wind turbine blade with different number of sections. In this table for easy understanding the sections with the same chord and twist values are highlighted with the same colors. Table 2 also tabulates the calculated angle of attack at each station.

Figure 2 shows the technical drawings of the blade geometries presented in Table 2, for a better visualization of the different concept wind turbine blades with different number of sections,

Figure 5 shows the Cl/Cd values (glide ratio) at the stations of selected concept wind turbine blades. In Figure 5 in each selected concept wind turbine blades figure we also plot the UAE Phase VI blade polar data for comparison. Also in this figure the big red and blue circles with dotted line encapsulates the polar data to see where the polar data concentrates.

Figure 6 shows the angle of attack range of selected concept wind turbine blades given in Table 2 on the lift & drag curve of the S809 airfoil. This figure helps us to see if the angle of attack range of a certain concept blade with a certain number of section falls in the stall region of the airfoil S809 or not.

After obtaining the concept wind turbine blades at the design speed through the optimization algorithm, by changing the wind speed and applying the BEM simulation, we obtain the power curve of each concept wind turbine blade. Figure 10 shows the power curve of all of the concept wind turbine blades together with the UAE Phase VI blade power curve for comparison.

First we run our simulation for a concept blade with 1 section only. As we mentioned earlier, in our calculations we have decided to always match the chord value in the last segment at the tip of the concept blade to the chord value at the tip of the UAE Phase VI blade. Because of this constraint, in a 1 section blade the chord from root to tip would have to be equal to the chord at the tip of the UAE Phase VI blade. As a result 1 section blade will be very thin in terms of chord length due to the constraint. In 1 section blade our algorithm only searches for the best twist angle that would offer the most aerodynamic power for the blade.

Table 2. UAE Phase VI and concept blade geometries and calculated angle of attack at the stations

a) UAE Phase VI blade

Delta R R_{i+1}-R_i (m)	i^{th} station	Radial Position (m)	Chord (m)	Twist (degree)	Angle of Attack (degree)
	R_1	1.258	0.737	20.05	12.9
0.264	R_2	1.522	0.710	14.04	13.6
0.276	R_3	1.798	0.682	9.67	13.6
0.277	R_4	2.075	0.654	6.75	13.1
0.277	R_5	2.352	0.626	4.84	12.5
0.276	R_6	2.628	0.598	3.48	11.8
0.277	R_7	2.905	0.570	2.40	11.2
0.276	R_8	3.181	0.542	1.51	10.6
0.277	R_9	3.458	0.514	0.76	10.2
0.277	R_10	3.735	0.486	0.09	9.9
0.037	R_11	3.772	0.483	0.00	9.7
0.239	R_12	4.011	0.459	-0.55	9.3
0.277	R_13	4.288	0.431	-1.11	8.8
0.277	R_14	4.565	0.403	-1.55	7.9
0.276	R_15	4.841	0.375	-1.84	5.9
0.189	R_16	5.030	0.356	-2.00	-

b) 1 section blade

Delta R R_{i+1}-R_i (m)	i^{th} station	Radial Position (m)	Chord (m)	Twist (degree)	Angle of Attack (degree)
	R_1	1.258	0.356	1.10	34.0
0.264	R_2	1.522	0.356	1.10	28.9
0.276	R_3	1.798	0.356	1.10	24.8
0.277	R_4	2.075	0.356	1.10	21.2
0.277	R_5	2.352	0.356	1.10	18.3
0.276	R_6	2.628	0.356	1.10	15.9
0.277	R_7	2.905	0.356	1.10	14.0
0.276	R_8	3.181	0.356	1.10	12.4
0.277	R_9	3.458	0.356	1.10	11.0
0.277	R_10	3.735	0.356	1.10	9.8
0.037	R_11	3.772	0.356	1.10	9.7
0.239	R_12	4.011	0.356	1.10	8.7
0.277	R_13	4.288	0.356	1.10	7.7
0.277	R_14	4.565	0.356	1.10	6.7
0.276	R_15	4.841	0.356	1.10	5.2
0.189	R_16	5.030	0.356	1.10	-

c) 2 section blade

Delta R R_{i+1}-R_i (m)	i^{th} station	Radial Position (m)	Chord (m)	Twist (degree)	Angle of Attack (degree)
	R_1	1.258	0.570	1.85	32.0
0.264	R_2	1.522	0.570	1.85	27.1
0.276	R_3	1.798	0.570	1.85	23.0
0.277	R_4	2.075	0.570	1.85	19.1
0.277	R_5	2.352	0.570	1.85	16.1
0.276	R_6	2.628	0.570	1.85	13.8
0.277	R_7	2.905	0.570	1.85	12.0
0.276	R_8	3.181	0.570	1.85	10.5
0.277	R_9	3.458	0.570	1.85	9.2
0.277	R_10	3.735	0.570	1.85	8.0
0.037	R_11	3.772	0.570	1.85	7.9
0.239	R_12	4.011	0.570	1.85	7.0
0.277	R_13	4.288	0.570	1.85	6.0
0.277	R_14	4.565	0.570	1.85	5.0
0	R_14	4.565	0.356	-1.76	9.0
0.276	R_15	4.841	0.356	-1.76	7.1
0.189	R_16	5.030	0.356	-1.76	-

d) 3 section blade

Delta R R_{i+1}-R_i (m)	i^{th} station	Radial Position (m)	Chord (m)	Twist (degree)	Angle of Attack (degree)
	R_1	1.258	0.682	11.42	22.0
0.264	R_2	1.522	0.682	11.42	16.3
0.276	R_3	1.798	0.682	11.42	12.2
0.277	R_4	2.075	0.682	11.42	9.3
0.277	R_5	2.352	0.682	11.42	7.0
0	R_5	2.352	0.515	0.85	17.5
0.276	R_6	2.628	0.515	0.85	15.2
0.277	R_7	2.905	0.515	0.85	13.2
0.276	R_8	3.181	0.515	0.85	11.7
0.277	R_9	3.458	0.515	0.85	10.3
0.277	R_10	3.735	0.515	0.85	9.1
0.037	R_11	3.772	0.515	0.85	9.0
0.239	R_12	4.011	0.515	0.85	8.1
0.277	R_13	4.288	0.515	0.85	7.0
0.277	R_14	4.565	0.515	0.85	5.9
0	R_14	4.565	0.356	-1.76	9.0
0.276	R_15	4.841	0.356	-1.76	7.1
0.189	R_16	5.030	0.356	-1.76	-

e) 4 section blade

Delta R R_{i+1}-R_i (m)	i^{th} station	Radial Position (m)	Chord (m)	Twist (degree)	Angle of Attack (degree)
	R_1	1.258	0.696	12.72	20.3
0.264	R_2	1.522	0.696	12.72	14.9
0.276	R_3	1.798	0.696	12.72	11.0
0.277	R_4	2.075	0.696	12.72	8.2
0	R_4	2.075	0.612	5.02	15.5
0.277	R_5	2.352	0.612	5.02	12.8
0.276	R_6	2.628	0.612	5.02	10.7
0.277	R_7	2.905	0.612	5.02	9.0
0	R_7	2.905	0.487	-0.14	14.4
0.276	R_8	3.181	0.487	-0.14	12.7
0.277	R_9	3.458	0.487	-0.14	11.4
0.277	R_10	3.735	0.487	-0.14	10.1
0.037	R_11	3.772	0.487	-0.14	10.0
0.239	R_12	4.011	0.487	-0.14	9.0
0.277	R_13	4.288	0.487	-0.14	8.0
0.277	R_14	4.565	0.487	-0.14	6.8
0	R_14	4.565	0.356	-1.76	9.0
0.276	R_15	4.841	0.356	-1.76	7.1
0.189	R_16	5.030	0.356	-1.76	-

f) 5 section blade

Delta R R_{i+1}-R_i (m)	i^{th} station	Radial Position (m)	Chord (m)	Twist (degree)	Angle of Attack (degree)
	R_1	1.258	0.710	14.61	18.0
0.264	R_2	1.522	0.710	14.61	13.0
0.276	R_3	1.798	0.710	14.61	9.3
0	R_3	1.798	0.640	6.85	16.9
0.277	R_4	2.075	0.640	6.85	13.5
0.277	R_5	2.352	0.640	6.85	11.0
0.276	R_6	2.628	0.640	6.85	9.0
0	R_6	2.628	0.529	1.01	14.9
0.277	R_7	2.905	0.529	1.01	13.0
0.276	R_8	3.181	0.529	1.01	11.4
0.277	R_9	3.458	0.529	1.01	10.1
0.277	R_10	3.735	0.529	1.01	8.9
0.037	R_11	3.772	0.529	1.01	8.8
0.239	R_12	4.011	0.529	1.01	7.9
0	R_12	4.011	0.417	-1.69	10.8
0.277	R_13	4.288	0.417	-1.69	9.7
0.277	R_14	4.565	0.417	-1.69	8.5
0.276	R_15	4.841	0.417	-1.69	6.6
0	R_15	4.841	0.356	-1.93	7.3
0.189	R_16	5.030	0.356	-1.93	-

g) 6 section blade

Delta R R_{i+1}-R_i (m)	i^{th} station	Radial Position (m)	Chord (m)	Twist (degree)	Angle of Attack (degree)
	R_1	1.258	0.710	14.61	18.0
0.264	R_2	1.522	0.710	14.61	13.0
0.276	R_3	1.798	0.710	14.61	9.3
0	R_3	1.798	0.654	8.41	15.2
0.277	R_4	2.075	0.654	8.41	12.0
0.277	R_5	2.352	0.654	8.41	9.6
0	R_5	2.352	0.584	3.71	14.2
0.276	R_6	2.628	0.584	3.71	12.0
0.277	R_7	2.905	0.584	3.71	10.3
0.276	R_8	3.181	0.584	3.71	8.8
0	R_8	3.181	0.487	-0.13	12.7
0.277	R_9	3.458	0.487	-0.13	11.4
0.277	R_10	3.735	0.487	-0.13	10.1
0.037	R_11	3.772	0.487	-0.13	10.0
0.239	R_12	4.011	0.487	-0.13	9.0
0.277	R_13	4.288	0.487	-0.13	8.0
0	R_13	4.288	0.403	-1.84	9.9
0.277	R_14	4.565	0.403	-1.84	8.7
0.276	R_15	4.841	0.403	-1.84	6.8
0	R_15	4.841	0.356	-1.93	7.3
0.189	R_16	5.030	0.356	-1.93	-

h) 7 section blade

Delta R R_{i+1}-R_i (m)	i^{th} station	Radial Position (m)	Chord (m)	Twist (degree)	Angle of Attack (degree)
	R_1	1.258	0.710	14.61	18.0
0.264	R_2	1.522	0.710	14.61	13.0
0.276	R_3	1.798	0.710	14.61	9.3
0	R_3	1.798	0.654	8.41	15.2
0.277	R_4	2.075	0.654	8.41	12.0
0.277	R_5	2.352	0.654	8.41	9.6
0	R_5	2.352	0.598	3.92	13.9
0.276	R_6	2.628	0.598	3.92	11.7
0.277	R_7	2.905	0.598	3.92	10.0
0	R_7	2.905	0.527	1.03	13.0
0.276	R_8	3.181	0.527	1.03	11.4
0.277	R_9	3.458	0.527	1.03	10.1
0.277	R_10	3.735	0.527	1.03	8.9
0.037	R_11	3.772	0.527	1.03	8.8
0	R_11	3.772	0.443	-1.06	11.1
0.239	R_12	4.011	0.443	-1.06	10.1
0.277	R_13	4.288	0.443	-1.06	9.0
0.277	R_14	4.565	0.443	-1.06	7.8
0	R_14	4.565	0.389	-1.84	8.8
0.276	R_15	4.841	0.389	-1.84	6.9
0	R_15	4.841	0.356	-1.93	7.3
0.189	R_16	5.030	0.356	-1.93	-

i) 8 section blade

Delta R R_{i+1}-R_i (m)	i^{th} station	Radial Position (m)	Chord (m)	Twist (degree)	Angle of Attack (degree)
	R_1	1.258	0.724	16.77	15.6
0.264	R_2	1.522	0.724	16.77	11.0
0	R_2	1.522	0.696	12.72	14.9
0.276	R_3	1.798	0.696	12.72	11.0
0	R_3	1.798	0.654	8.41	15.2
0.277	R_4	2.075	0.654	8.41	12.0
0.277	R_5	2.352	0.654	8.41	9.6
0	R_5	2.352	0.598	3.92	13.9
0.276	R_6	2.628	0.598	3.92	11.7
0.277	R_7	2.905	0.598	3.92	10.0
0	R_7	2.905	0.527	1.03	13.0
0.276	R_8	3.181	0.527	1.03	11.4
0.277	R_9	3.458	0.527	1.03	10.1
0.277	R_10	3.735	0.527	1.03	8.9
0.037	R_11	3.772	0.527	1.03	8.8
0	R_11	3.772	0.443	-1.06	11.1
0.239	R_12	4.011	0.443	-1.06	10.1
0.277	R_13	4.288	0.443	-1.06	9.0
0.277	R_14	4.565	0.443	-1.06	7.8
0	R_14	4.565	0.389	-1.84	8.8
0.276	R_15	4.841	0.389	-1.84	6.9
0	R_15	4.841	0.356	-1.93	7.3
0.189	R_16	5.030	0.356	-1.93	-

j) 9 section blade

Delta R R_{i+1}-R_i (m)	i^{th} station	Radial Position (m)	Chord (m)	Twist (degree)	Angle of Attack (degree)
	R_1	1.258	0.724	16.77	15.6
0.264	R_2	1.522	0.724	16.77	11.0
0	R_2	1.522	0.696	12.72	14.9
0.276	R_3	1.798	0.696	12.72	11.0
0	R_3	1.798	0.668	9.58	14.0
0.277	R_4	2.075	0.668	9.58	10.9
0	R_4	2.075	0.626	5.79	14.6
0.277	R_5	2.352	0.626	5.79	12.0
0.276	R_6	2.628	0.626	5.79	10.0
0	R_6	2.628	0.570	2.93	12.8
0.277	R_7	2.905	0.570	2.93	11.0
0.276	R_8	3.181	0.570	2.93	9.5
0	R_8	3.181	0.501	0.16	12.4
0.277	R_9	3.458	0.501	0.16	11.0
0.277	R_10	3.735	0.501	0.16	9.8
0.037	R_11	3.772	0.501	0.16	9.7
0.239	R_12	4.011	0.501	0.16	8.7
0	R_12	4.011	0.431	-1.24	10.3
0.277	R_13	4.288	0.431	-1.24	9.2
0.277	R_14	4.565	0.431	-1.24	8.0
0	R_14	4.565	0.389	-1.84	8.8
0.276	R_15	4.841	0.389	-1.84	6.9
0	R_15	4.841	0.356	-1.93	7.3
0.189	R_16	5.030	0.356	-1.93	-

k) 10 section blade

Delta R R_{i+1}-R_i (m)	i^{th} station	Radial Position (m)	Chord (m)	Twist (degree)	Angle of Attack (degree)
	R_1	1.258	0.724	16.77	15.6
0.264	R_2	1.522	0.724	16.77	11.0
0	R_2	1.522	0.696	12.72	14.9
0.276	R_3	1.798	0.696	12.72	11.0
0	R_3	1.798	0.668	9.58	14.0
0.277	R_4	2.075	0.668	9.58	10.9
0	R_4	2.075	0.626	5.79	14.6
0.277	R_5	2.352	0.626	5.79	12.0
0.276	R_6	2.628	0.626	5.79	10.0
0	R_6	2.628	0.570	2.93	12.8
0.277	R_7	2.905	0.570	2.93	11.0
0.276	R_8	3.181	0.570	2.93	9.5
0	R_8	3.181	0.513	0.49	12.0
0.277	R_9	3.458	0.513	0.49	10.6
0.277	R_10	3.735	0.513	0.49	9.5
0.037	R_11	3.772	0.513	0.49	9.3
0	R_11	3.772	0.457	-1.05	11.0
0.239	R_12	4.011	0.457	-1.05	10.0
0.277	R_13	4.288	0.457	-1.05	8.9
0	R_13	4.288	0.417	-1.55	9.6
0.277	R_14	4.565	0.417	-1.55	8.4
0	R_14	4.565	0.389	-1.84	8.8
0.276	R_15	4.841	0.389	-1.84	6.9
0	R_15	4.841	0.356	-1.93	7.3
0.189	R_16	5.030	0.356	-1.93	-

l) 11 section blade

Delta R R_{i+1}-R_i (m)	i^{th} station	Radial Position (m)	Chord (m)	Twist (degree)	Angle of Attack (degree)
	R_1	1.258	0.724	16.77	15.6
0.264	R_2	1.522	0.724	16.77	11.0
0	R_2	1.522	0.696	12.72	14.9
0.276	R_3	1.798	0.696	12.72	11.0
0	R_3	1.798	0.668	9.58	14.0
0.277	R_4	2.075	0.668	9.58	10.9
0	R_4	2.075	0.640	6.75	13.6
0.277	R_5	2.352	0.640	6.75	11.1
0	R_5	2.352	0.612	4.78	13.0
0.276	R_6	2.628	0.612	4.78	10.9
0	R_6	2.628	0.570	2.93	12.8
0.277	R_7	2.905	0.570	2.93	11.0
0.276	R_8	3.181	0.570	2.93	9.5
0	R_8	3.181	0.513	0.49	12.0
0.277	R_9	3.458	0.513	0.49	10.6
0.277	R_10	3.735	0.513	0.49	9.5
0.037	R_11	3.772	0.513	0.49	9.3
0	R_11	3.772	0.457	-1.05	11.0
0.239	R_12	4.011	0.457	-1.05	10.0
0.277	R_13	4.288	0.457	-1.05	8.9
0	R_13	4.288	0.417	-1.55	9.6
0.277	R_14	4.565	0.417	-1.55	8.4
0	R_14	4.565	0.389	-1.84	8.8
0.276	R_15	4.841	0.389	-1.84	6.9
0	R_15	4.841	0.356	-1.93	7.3
0.189	R_16	5.030	0.356	-1.93	-

Table 2. UAE Phase VI and concept blade geometries and calculated angle of attack at the stations (continued)

m) 12 section blade

Delta R R_{i+1}-R_i (m)	i^{th} station	Radial Position (m)	Chord (m)	Twist (degree)	Angle of Attack (degree)
	R_1	1.258	0.724	16.77	15.6
0.264	R_2	1.522	0.724	16.77	11.0
0	R_2	1.522	0.696	12.72	14.9
0.276	R_3	1.798	0.696	12.72	11.0
0	R_3	1.798	0.668	9.58	14.0
0.277	R_4	2.075	0.668	9.58	10.9
0	R_4	2.075	0.640	6.75	13.6
0.277	R_5	2.352	0.640	6.75	11.1
0	R_5	2.352	0.612	4.78	13.0
0.276	R_6	2.628	0.612	4.78	10.9
0	R_6	2.628	0.584	3.48	12.2
0.277	R_7	2.905	0.584	3.48	10.5
0	R_7	2.905	0.542	1.41	12.5
0.276	R_8	3.181	0.542	1.41	11.0
0.277	R_9	3.458	0.542	1.41	9.7
0	R_9	3.458	0.499	0.17	11.0
0.277	R_10	3.735	0.499	0.17	9.8
0.037	R_11	3.772	0.499	0.17	9.7
0	R_11	3.772	0.457	-1.05	11.0
0.239	R_12	4.011	0.457	-1.05	10.0
0.277	R_13	4.288	0.457	-1.05	8.9
0	R_13	4.288	0.417	-1.55	9.6
0.277	R_14	4.565	0.417	-1.55	8.4
0	R_14	4.565	0.389	-1.84	8.8
0.276	R_15	4.841	0.389	-1.84	6.9
0	R_15	4.841	0.356	-1.93	7.3
0.189	R_16	5.030	0.356	-1.93	-

n) 13 section blade

Delta R R_{i+1}-R_i (m)	i^{th} station	Radial Position (m)	Chord (m)	Twist (degree)	Angle of Attack (degree)
	R_1	1.258	0.724	16.77	15.6
0.264	R_2	1.522	0.724	16.77	11.0
0	R_2	1.522	0.696	12.72	14.9
0.276	R_3	1.798	0.696	12.72	11.0
0	R_3	1.798	0.668	9.58	14.0
0.277	R_4	2.075	0.668	9.58	10.9
0	R_4	2.075	0.640	6.75	13.6
0.277	R_5	2.352	0.640	6.75	11.1
0	R_5	2.352	0.612	4.78	13.0
0.276	R_6	2.628	0.612	4.78	10.9
0	R_6	2.628	0.584	3.48	12.2
0.277	R_7	2.905	0.584	3.48	10.5
0	R_7	2.905	0.556	2.40	11.6
0.276	R_8	3.181	0.556	2.40	10.1
0	R_8	3.181	0.528	1.13	11.3
0.277	R_9	3.458	0.528	1.13	10.0
0	R_9	3.458	0.499	0.17	11.0
0.277	R_10	3.735	0.499	0.17	9.8
0.039	R_11	3.772	0.499	0.17	9.7
0	R_11	3.772	0.457	-1.05	11.0
0.239	R_12	4.011	0.457	-1.05	10.0
0.277	R_13	4.288	0.457	-1.05	8.9
0	R_13	4.288	0.417	-1.55	9.6
0.277	R_14	4.565	0.417	-1.55	8.4
0	R_14	4.565	0.389	-1.84	8.8
0.276	R_15	4.841	0.389	-1.84	6.9
0	R_15	4.841	0.356	-1.93	7.3
0.189	R_16	5.030	0.356	-1.93	-

o) 14 section blade

Delta R R_{i+1}-R_i (m)	i^{th} station	Radial Position (m)	Chord (m)	Twist (degree)	Angle of Attack (degree)
	R_1	1.258	0.724	16.77	15.6
0.264	R_2	1.522	0.724	16.77	11.0
0	R_2	1.522	0.696	12.72	14.9
0.276	R_3	1.798	0.696	12.72	11.0
0	R_3	1.798	0.668	9.58	14.0
0.277	R_4	2.075	0.668	9.58	10.9
0	R_4	2.075	0.640	6.75	13.6
0.277	R_5	2.352	0.640	6.75	11.1
0	R_5	2.352	0.612	4.78	13.0
0.276	R_6	2.628	0.612	4.78	10.9
0	R_6	2.628	0.584	3.48	12.2
0.277	R_7	2.905	0.584	3.48	10.5
0	R_7	2.905	0.556	2.40	11.6
0.276	R_8	3.181	0.556	2.40	10.1
0	R_8	3.181	0.528	1.13	11.3
0.277	R_9	3.458	0.528	1.13	10.0
0	R_9	3.458	0.499	0.17	11.0
0.277	R_10	3.735	0.499	0.17	9.8
0.037	R_11	3.772	0.499	0.17	9.7
0	R_11	3.772	0.471	-0.55	10.4
0.239	R_12	4.011	0.471	-0.55	9.5
0	R_12	4.011	0.445	-1.08	10.1
0.277	R_13	4.288	0.445	-1.08	9.0
0	R_13	4.288	0.417	-1.55	9.6
0.277	R_14	4.565	0.417	-1.55	8.4
0	R_14	4.565	0.389	-1.84	8.8
0.276	R_15	4.841	0.389	-1.84	6.9
0	R_15	4.841	0.356	-1.93	7.3
0.189	R_16	5.030	0.356	-1.93	-

p) 15 section blade

Delta R R_{i+1}-R_i (m)	i^{th} station	Radial Position (m)	Chord (m)	Twist (degree)	Angle of Attack (degree)
	R_1	1.258	0.724	16.77	15.6
0.264	R_2	1.522	0.724	16.77	11.0
0	R_2	1.522	0.696	12.72	14.9
0.276	R_3	1.798	0.696	12.72	11.0
0	R_3	1.798	0.668	9.58	14.0
0.277	R_4	2.075	0.668	9.58	10.9
0	R_4	2.075	0.640	6.75	13.6
0.277	R_5	2.352	0.640	6.75	11.1
0	R_5	2.352	0.612	4.78	13.0
0.276	R_6	2.628	0.612	4.78	10.9
0	R_6	2.628	0.584	3.48	12.2
0.277	R_7	2.905	0.584	3.48	10.5
0	R_7	2.905	0.556	2.40	11.6
0.276	R_8	3.181	0.556	2.40	10.1
0	R_8	3.181	0.528	1.13	11.3
0.277	R_9	3.458	0.528	1.13	10.0
0	R_9	3.458	0.500	0.17	11.0
0.277	R_10	3.735	0.500	0.17	9.8
0	R_10	3.735	0.485	0.00	10.0
0.039	R_11	3.772	0.485	0.00	9.9
0	R_11	3.772	0.471	-0.55	10.4
0.239	R_12	4.011	0.471	-0.55	9.5
0	R_12	4.011	0.445	-1.08	10.1
0.277	R_13	4.288	0.445	-1.08	9.0
0	R_13	4.288	0.417	-1.55	9.6
0.277	R_14	4.565	0.417	-1.55	8.4
0	R_14	4.565	0.389	-1.84	8.8
0.276	R_15	4.841	0.389	-1.84	6.9
0	R_15	4.841	0.356	-1.93	7.3
0.189	R_16	5.030	0.356	-1.93	-

As can be seen in Figure 2-b, 1 section blade is actually very thin compared to the UAE Phase VI blade also shown in Figure 2-a. Since in a 1 section blade there is no variation in the twist value along the blade spanwise, through the whole blade the angle of attack range of the blade is very wide as seen in Figure 6-b and Table 2-b. When we look at the polar data shown in Figure 5-b we can see that at some stations 1 section blade operates with very low glide ratio which is not very efficient. From Figure 5-b and Figure 6-b it is clear that most part of the 1 section blade is operating in a condition that is not aerodynamically very efficient, however this is inevitable for a 1 section blade since the blade does not have a twist. Since 1 section blade is very thin in terms of chord length as shown in Figure 2-b, the blade has a low power curve as seen in Figure 10. At all wind speeds, the power that 1 section blade can generate is lower than that of UAE Phase VI blade.

We then consider a 2 section blade. Since in a 2 section blade we have two different twist values in each section as shown in the technical drawing in Figure 2-c, the angle of attack range is better than that of a 1 section blade as seen in Figure 6-c and Table 2-c even though the improvement is small. As it is seen in Figure 5-c, compared to 1 section blade there is a slight improvement in the polar values also. In Figure 5-c one can notice that small blue symbols start to move to the left towards the optimum point compared to the blue symbols in 1 section blade in Figure 5-b. Although with a 2 section blade there is a definite aerodynamic improvement compared to a 1 section blade, still a 2 section blade is far from being an efficient wind turbine blade. As seen in Figure 2-c, the first section close to the hub has a thicker chord and also the length of this section is very long covering 13 segments of the total 15 segments, thus the blade looks very much like a thick large blade with a thinner small blade attached to it at the tip. If we look at the power curve of 2 section blade in Figure 10, we see that up to 10 m/s wind speed this blade can generate less power than that of the UAE Phase VI blade, however above 10 m/s it generates more power.

Then similarly we continue and consider a 3 section blade. Among the 91 different possibilities for a 3 section blade, iterating on every possible twist angle at each 3 stations, the geometry given in Figure 2-d and Table 2-d offers the most power. Looking at the angle of attack range in the segments of this 3 section blade in Figure 6-d, we can see that there is more improvement compared to 1 and 2 section blades such that the angle of attack range gets narrow with less portion being after the stall peak. We can also see this improvement in the polar data as seen in Figure 5-d. Looking at Figure 5-c and 5-d one can easily notice that as the number of section increases from 2 to 3, the glide ratio at the stations gets much better and the blue symbols move to the left towards the optimum point very quickly. As seen in Figure 5-d the blue symbols are scattered with a big encapsulated dotted circle compared to the red symbols which are more concentrated to each other with a smaller red dotted circle. As we increase from 2 section to 3 section blade, in Figure 10 we see that the power curve of 3 section blade is converging towards the power curve of the UAE Phase VI blade. We will not discuss each of the blades with different number of sections separately. Looking at the sequences in Figure 5 and 6, when the number of sections increases in the wind turbine blade, the solutions of the concept blades converge towards the solution of the UAE Phase VI blade. For example in Figure 6 as the number of sections in the blade increases, in the segments throughout

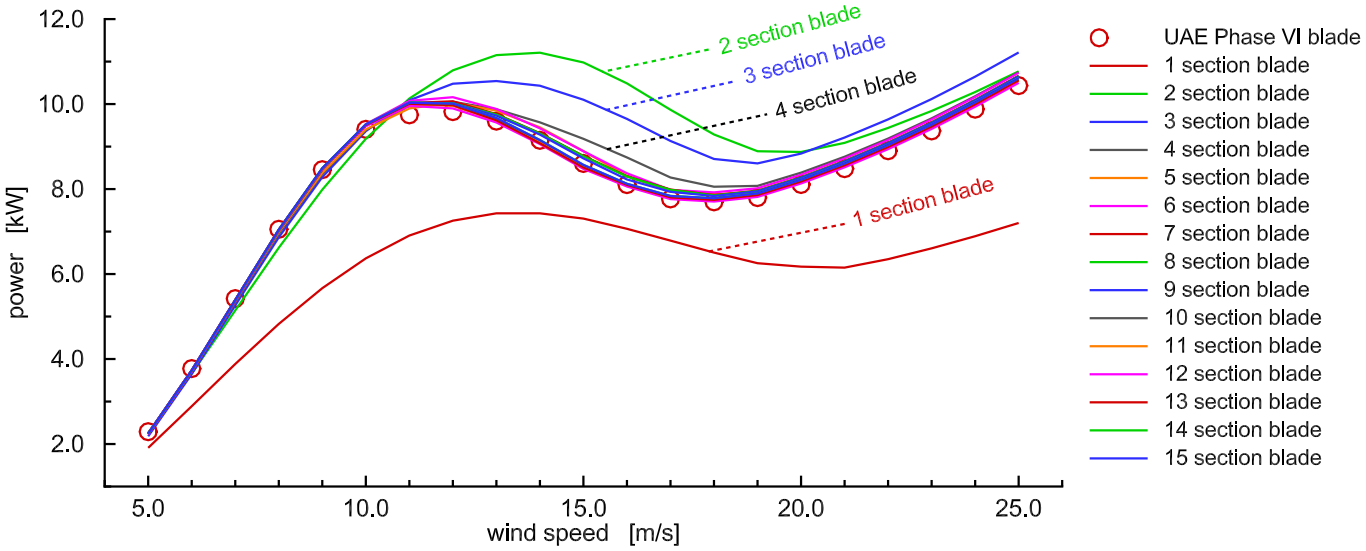

Fig. 10. Power curve of the concept wind turbine blades compared and the UAE Phase VI blade

the blade, the angle of attack range gets smaller and converges towards the ramp in the lift curve before the stall peak. We see the same behavior in the polar data also, such that in Figure 5 as the number of section increases the polar data in the stations move towards left and concentrate around the highest glide ratio which offers the best aerodynamic condition. In Figure 10 almost all of the concept blades with 5 section and above have more or less the same power curve with each other matching the power curve of the UAE Phase VI blade. The largest considered in this study, a 15 section blade is very close to the UAE Phase VI blade in many aerodynamic parameters.

Figure 11 shows the chord and twist distribution along the span of 1, 3, 5 and 15 section blades together with that of the UAE Phase VI blade. In this figure one can notice that the twist distribution that our optimization algorithm suggests for the sections in the blades matches with the twist distribution of the original UAE Phase VI blade very good in a piecewise manner.

In this study we have performed a preliminary analysis of a concept wind turbine blade that consists of sections with constant chord and twist values using Blade Element Momentum (BEM) method together with an optimization algorithm. The straight sections can easily be manufactured by pultrusion process with significantly decrease in the cost, with consistent high quality and also without any hand laboring, eliminating the human related manufacturing defects. With the pultrusion process the blades can be manufactured all together with the spar cap, shear web and the airfoil shell integrated as one as illustrated in Figure 12. This will also eliminate the bonding related manufacturing defects. Besides due to the nature of its design, sectioned wind turbine blades offer a possibility of modular blades. Since each section of the blade is manufactured separately, they can be transported to the wind turbine site also separately very easily and cheaply eliminating the existing logistics challenges faced in transporting long blades and then they can be assembled on the site using a mechanical joint in between the two sections.

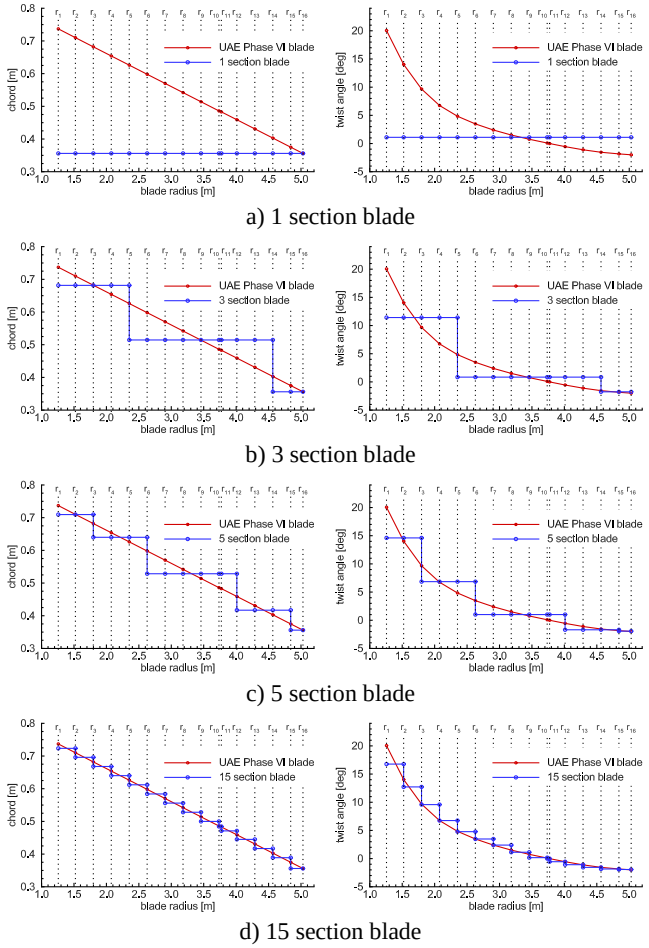

a) 1 section blade

b) 3 section blade

c) 5 section blade

d) 15 section blade

Fig. 11. Spanwise chord and twist angle distribution

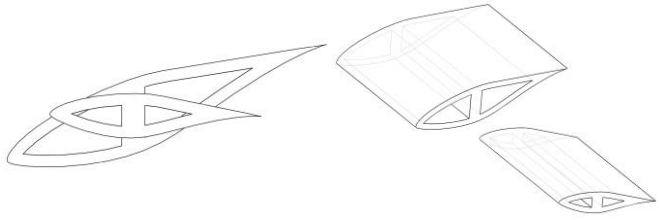

Fig. 12. Illustrations of the concept wind turbine blade

Since transportation of smaller length sections are easier and cheaper, having more sections in a blade is preferable in terms of transportation. From transportation point of view solely, in our case the best choice seems to have a 15 section blade among the concept wind turbine blades in this study. However on the other side, more sections would require more dies for pultrusion which indicates an increase in initial die cost. We note that in the considered concept wind turbine blades there is a step change in the chord and twist values at the junction of any two sections. We also note that we have used a BEM simulation in our preliminary analysis. As the wind turbine blade rotates, due to the centrifugal effects there will be a cross-flow in radial direction on the blade. In the considered concept blades since there are step changes in the geometry in radial direction, there may be some aerodynamic losses at the junctions and a BEM simulation does not take the aerodynamic losses that might occur at the junctions into account. For this reason we do not know the magnitude of the aerodynamic losses that might occur at the junctions. Only a detailed CFD simulation or an experiment would give an idea on the magnitude of the corresponding aerodynamic losses. We would like to point out that a BEM analysis can serve for a preliminary analysis to search the applicability of the idea however it is clear that further and detailed analysis are needed for a better understanding of the concept. Anyhow the aerodynamic losses that might occur at the junction of sections is not in the scope of this study.

In order to decrease the potential aerodynamic losses that might occur at the junctions, one can suggest to have minimum number of sections in the blade such that there will be less number of step changes in the radial direction although another one can argue that when the number of sections are large, the magnitude of the step changes are small therefore the aerodynamic losses can be less if maximum number of sections is chosen. In their study Lanzafame and Messina [19] have proposed to use a winglet to decrease the aerodynamic losses that might occur due to step change in the geometry. Winglets are wing tip devices that are used to increase the aerodynamic efficiency of the modern airplanes. However when winglets are used on the wind turbine blades along the span, depending on the number of winglets used, they may create additional drag since winglets usually have comparable sizes. Since our aim is to minimize the possible aerodynamic losses that might occur at the junction of the sections due to spanwise flow we think that a wing fence (or sometimes called stall fence or boundary layer fence) would serve better to this purpose rather than a winglet because a wing fence is smaller than a winglet in size which then would create less drag. We also note that in order to decrease the aerodynamic losses, as it is suggested in [21], at the junction of any two sections a tapered and twisted small section can be used to eliminate the discontinuity and have a smoother transition from one section to another.

Another potential drawback of the concept wind turbine blade might possibly be comparably higher aerodynamic sound emission. However as described in [35], with further studies, possible aerodynamic noise can be reduced by several shape design options and blade add-ons.

Finally we would like to note that the magnitude of any drawbacks of the concept wind turbine blade can be reduced with further studies.

5. Conclusions

In this study the preliminary analysis of a concept wind turbine blade is presented. The concept wind turbine blade has several sections with having different constant chord and twist values in each section. In order to set the chord and twist values at each section an optimization algorithm is presented. Using this algorithm several different concept wind turbine blades with different number of sections are obtained for the UAE Phase VI experiment. The aerodynamic efficiency of these different concept wind turbine blades are compared with the original UAE Phase VI blade. The results show that the concept wind turbine blades have good aerodynamic efficiencies with having almost the same power output with the original UAE Phase VI blade. The concept wind turbine blade offers manufacturing of the wind turbine blades with high quality using cheaper and easier manufacturing techniques eliminating the commonly faced manufacturing defects. Furthermore the concept wind turbine blade naturally offers a possibility of wind turbine blades to have modular design.

References

[1] US Department of Energy web page [accessed August 2018]
https://www.energy.gov/maps/map-projected-growth-wind-industry-now-until-2050

[2] Mohamed MH, Wetzel KK, (2006), "3D woven carbon/glass hybrid spar cap for wind turbine rotor blade", Journal of Solar Energy Engineering 128:562–573
https://doi.org/10.1115/1.2349543

[3] Griffin DA, Malkin MC, (2011), "Lessons Learned from Recent Blade Failures: Primary Causes and Risk-Reducing Technologies", 49th AIAA Aerospace Sciences Meeting including the New Horizons Forum and Aerospace Exposition, AIAA 2011-259
https://doi.org/10.2514/6.2011-259

[4] Mishnaevsky L, Branner K, Petersen HN, Beauson J, McGugan M, Sørensen BF, (2017), "Materials for Wind Turbine Blades: An Overview", Materials, 10:1285
https://doi.org/10.3390/ma10111285

[5] Sørensen BF, Jørgensen E, Debel CP, Jensen FM, Jensen HM, Jacobsen TK, Halling K, (2004), "Improved design of large wind turbine blade of fibre composites based on studies of scale effects (Phase 1). Summary Report", Riso-R1390(EN), Risø National Laboratory, Denmark
http://orbit.dtu.dk/fedora/objects/orbit:90493/datastreams/file_7702048/content

[6] Sheng S, (2013), "Report on Wind Turbine Subsystem Reliability - A Survey of Various Databases", NREL Paper, NREL/PR-5000-59111 https://www.nrel.gov/docs/fy13osti/59111.pdf

[7] Windpower Monthly magazine web page [accessed August 2018] http://www.windpowermonthly.com/article/1347145/annual-blade-failures-estimated-around-3800

[8] Suzlon company web page [accessed August 2018] http://www.suzlon.com/pressrelease/pressrelease_detail/256-suzlon-completes-blade-retrofit-program/2010

[9] Yang W, Sheng S, Court R, (2012), "Operational-Condition-Independent Criteria Dedicated to Monitoring Wind Turbine Generators", NREL Paper, NREL/CP-5000-55195 https://www.nrel.gov/docs/fy12osti/55195.pdf

[10] Jensen FM, Kling A, Sørensen JD, (2012), "Change in failure type when wind turbine blades scale-up", Sandia Wind Turbine Workshop 2012 http://energy.sandia.gov/wp-content//gallery/uploads/2B-A-1-Jensen1.pdf

[11] Mishnaevsky Jr, (2011), "Composite materials in wind energy technology, Thermal to Mechanical Energy Conversion: Engines and Requirements", EOLSS Publishers, Oxford, UK https://www.eolss.net/sample-chapters/C08/E3-11-42.pdf

[12] Power magazine web page [accessed August 2018] http://www.powermag.com/new-design-tool-improves-manufacture-of-composite-wind-turbine-blades/

[13] CompositesWorld magazine web page [accessed August 2018] https://www.compositesworld.com/articles/wind-blade-spar-caps-pultruded-to-perfection

[14] Schwartz MM, (1997), "Composite Materials - Processing. Fabrication, and Applications", Vol. 2. Prentice Hall PTR, ISBN:9780133000399 http://catalogue.pearsoned.co.uk/educator/product/Composite-Materials-Vol-II-Processing-Fabrication-and-Applications/9780133000399.page

[15] National Research Council, (1991), "Assessment of Research Needs for Wind Turbine Rotor Materials Technology", The National Academies Press, ISBN:9780309044790 https://doi.org/10.17226/1824

[16] Migliore PG, Cheney MC, (2000), "Feasibility Study of Pultruded Blades for Wind Turbine Rotors", NREL Paper, NREL/CP-500-27506 https://www.nrel.gov/docs/fy00osti/27506.pdf

[17] Cheney MC, Olsen T, Quandt G, Arcidiacono P, (1999), "Analysis and Tests of Pultruded Blades for Wind Turbine Rotors", NREL Paper, NREL/SR-500-25949 https://www.nrel.gov/docs/fy99osti/25949.pdf

[18] Cairns D, Skramstad J, Ashwill T, (2000), "Resin Transfer Molding and Wind Turbine Blade Construction", Sandia National Laboratories Technical Report, SAND99-3047 https://windpower.sandia.gov/other/SAND-993047.pdf

[19] Lanzafame R, Messina M, (2009), "Design and performance of a double-pitch wind turbine with non-twisted blades", Renewable Energy, 34:1413-1420 http://dx.doi.org/10.1016/j.renene.2008.09.004

[20] Hand MM, Simms DA, Fingersh LJ, Jager DW, Cotrell JR, Schreck S, Larwood SM, (2001), "Unsteady Aerodynamics Experiment Phase VI: Wind Tunnel Test Configurations and Available Data Campaigns", NREL Report, NREL/TP-500-29955 http://www.nrel.gov/docs/fy02osti/29955.pdf

[21] Smart Blade GmbH, "Modulares Rotorblatt für eine Windkraftanlage", DE102009023001A1, German Patent and Trade Mark Office 2010-12-02 https://register.dpma.de/DPMAregister/pat/PatSchrifteneinsicht?docId=DE102009023001A1

[22] Burton T, Sharpe D, Jenkins N, Bassanyi E, (2001), "Wind Energy Handbook", John Wiley & Sons Ltd. ISBN:9780470699751 http://dx.doi.org/10.1002/9781119992714

[23] Manwell JF, McGowan JG, Rogers AL, (2002), "Wind Energy Explained: Theory, Design and Application", John Wiley & Sons Ltd. ISBN:9780470015001 http://dx.doi.org/10.1002/9781119994367

[24] Hansen MOL, (2008), "Aerodynamics of Wind Turbines", Earthscan Publications Ltd. ISBN:9781844074389 https://www.routledge.com/products/9781844074389

[25] Koç E, Günel O, Yavuz T, (2016), "Comparison of Qblade and CFD results for small-scaled horizontal axis wind turbine analysis," 2016 IEEE International Conference on Renewable Energy Research and Applications (ICRERA), Birmingham, pp. 204-209. https://doi.org/10.1109/ICRERA.2016.7884538

[26] Viterna LA, Janetzke DC, (1982), "Theoretical and Experimental Power from Large Horizontal-Axis Wind Turbines", NASA Lewis Research Center Technical Report, NASA TM-82944 http://ntrs.nasa.gov/archive/nasa/casi.ntrs.nasa.gov/19820025954.pdf

[27] Montgomerie B, (2004), "Methods for Root Effects, Tip Effects and Extending the Angle of Attack to ±180 with Application to Aerodynamics for Blades on Wind Turbines and Propellers", Swedish Defence Research Agency Scientific Report, FOI-R--1305—SE [accessed August 2018] https://www.foi.se/rapportsammanfattning?reportNo=FOI-R--1305--SE

[28] Lindenburg C, (2003), "Investigation into Rotor Blade Aerodynamics", Energy research Centre of the Netherlands (ECN) Wind Energy publication, ECN-C--03-025
https://www.ecn.nl/publications/PdfFetch.aspx?nr=ECN-C--03-025

[29] Tangler J, Kocurek JD, (2005), "Wind Turbine Post-Stall Airfoil Performance Characteristics Guidelines for Blade-Element Momentum Methods", NREL Report, NREL/CP-500-36900
http://www.nrel.gov/docs/fy05osti/36900.pdf

[30] Spera DA, (2008), "Models of Lift and Drag Coeffi cients of Stalled and Unstalled Airfoils in Wind Turbines and Wind Tunnels", NASA Technical Report NASA/CR-2008-215434
http://ntrs.nasa.gov/archive/nasa/casi.ntrs.nasa.gov/20090001311.pdf

[31] Erturk E, AERODAS spreadsheet download web page [accessed August 2018]
http://www.cavityflow.com/aerodas.rar

[32] Giguère P, Selig MS, (1999), "Design of a Tapered and Twisted Blade for the NREL Combined Experiment Rotor", NREL Report, NREL/SR-500-26173
http://www.nrel.gov/docs/fy99osti/26173.pdf

[33] Tangler JL, (2002), "The Nebulous Art of UsingWind-Tunnel Airfoil Data for Predicting Rotor Performance", NREL Report, NREL/CP-500-31243
http://www.nrel.gov/docs/fy02osti/31243.pdf

[34] Yelmule MM, Anjuri ER, (2013), "CFD predictions of NREL Phase VI Rotor Experiments in NASA/AMES Wind tunnel", International Journal of Renewable Energy Research, 3:261-269
http://www.ijrer.org/ijrer/index.php/ijrer/article/view/570/pdf

[35] Oerlemans S, (2011), "Wind turbine noise: primary noise sources", National Aerospace Laboratory NLR Report, NLR-TP-2011-066
https://reports.nlr.nl/xmlui/bitstream/handle/10921/117/TP-2011-066.pdf